Nano Research
DOI 10.1007/s12274-016-1148-0
Research Article
ISSN 1998-0124
CN 11-5974/O4

The nucleation and growth of borophene on the Ag (111) surface

Shaogang Xu[1,2], Yujun Zhao[1], Jihai Liao[1], Xiaobao Yang[1] (✉), and Hu Xu[2] (✉)

[1] *Department of Physics, South China University of Technology, Guangzhou 510640, China*
[2] *Department of Physics, South University of Science and Technology of China, Shenzhen 518055, China*

Received: 7 April 2016
Revised: 8 May 2016
Accepted: 12 May 2016

KEYWORDS
borophene,
hexagonal vacancy,
nucleation mechanism,
first-principles calculations

ABSTRACT

B sheets have been intently studied, and various candidates with vacancies have been reported in theoretical investigations, including their possible growth on metal surfaces. However, a recent experiment reported that the borophene formed on a Ag (111) surface consisted of a buckled triangular lattice without vacancies. Our calculations propose a novel nucleation mechanism of B clusters and emphasize the B–Ag interaction in the growth process of borophene, demonstrating the structural evolution of triangular fragments with various profiles and vacancy distributions. Compared with the triangular lattice without vacancies, we have confirmed that the sheet energetically favored during the nucleation and growth is that containing 1/6 vacancies in a stripe pattern, whose scanning tunneling microscopy image is in better agreement with the experimental observation.

1 Introduction

Because of the multi-center bonds, B nanostructures have shown a striking evolution as the size increases, which has attracted both theoretical and experimental attention in the past decades [1–5]. Several planar or quasi-planar structures (B_{17-24}) with tetragonal or pentagonal defects have been determined experimentally [1], and B_{30} [4] and B_{36} with hexagonal vacancies can be considered the precursor of borophene [5]. Here, the nomenclature of borophene was initially proposed in Ref. [5] and refers to a graphene-like B sheet with vacancies. Theoretically, stable B sheets [6, 7] have been observed to form a triangular lattice with proper vacancies, leading to extensive theoretical studies that focus on the concentration and distribution of vacancies [8–12]. A recent study demonstrated that a metal atom could fill the vacancy, forming a vacancy-free metallo-borophene, indicating that a vacancy is necessary on borophenes, where a metal atom should provide the electron needed [13].

The multi-center bonds highly depend on the atomic coordination, which might have a dramatic effect on the structural stabilities of B nanostructures. Theoretical investigations have predicted that possible B sheets can be synthesized on a metal surface (e.g., Cu, Ag,

Address correspondence to Xiaobao Yang, scxbyang@scut.edu.cn; Hu Xu, xu.h@sustc.edu.cn

and Au), indicating that the stable sheet with specific concentration and distribution of vacancies would change with the substrate [14–16]. Thin B films were experimentally observed on Cu surfaces with a mixture of B and boron oxide powders as the B source, where the monolayer of B_{28} comprises B_{12} icosahedrons and B_2 dumbbells [17]. Notably, the borophene with one atom-thick was experimentally observed on a Ag (111) surface using a solid B atomic source. This simple B sheet was suggested to consist of a buckled triangular lattice with no vacancies [18], which is in contrast to the previous theoretically predicted stable configurations of borophene on a Ag (111) surface [16].

To provide a better understanding of the growth of borophene, in this study, we theoretically investigated the possible B nucleation on the Ag (111) surface based on first-principles calculations. Surprisingly, we observed that small B clusters ($B_{1–3}$) deposited on the Ag surface would penetrate into the second layer without an energy barrier and further expel Ag atoms on top to form Ag vacancies, similar to the case of silicene growth on a Ag (111) surface [19]. The results of our simulations provide a clear picture of the nucleation and growth of borophene, where the B–Ag interaction is dominant in stabilizing the zigzag edge of B nanostructures and further induces vacancies in a stripe pattern. Calculations of the minimum energy paths and simulations of scanning tunneling microscopy (STM) images were also performed to explain the experimental observations.

2 Computational methods

The first-principles calculations of B nucleation and growth were based on density functional theory (DFT) implemented in the Vienna *ab initio* simulation package (VASP) method [20, 21]. The climbing image nudged elastic band method (CI-NEB) was used to search the energy barriers and reaction pathways [22]. Based on high-throughput screening with a congruence check [23], various configurations of B nanostructures were considered to model the nucleation on the Ag (111) surface, where the formation energies E_{form} were defined to describe the structural stabilities of B nanostructures. For the B nanostructures adsorbed or embedded in the Ag(111) first layer, we defined the formation energy per B atom as $E_{form} = \frac{1}{n}(E_{tot} + m \times E_{Ag} - E_{sub} - n \times E_B)$. Here, E_{Ag} is the energy per atom of the edge atoms on the Ag (111) surface (the total energy difference between the Ag slab and Ag slab with an edge Ag atom vacancy, whose absolute value is only slightly smaller than the per atom of Ag bulk); m is the number of expelled Ag atoms (m = 0 for adsorption without expelling Ag atoms); E_B is the energy per atom in the B solid of the α phase; n is the number of B atoms in the B monolayer or B_n cluster. Under such definitions, the configuration with a smaller E_{form} is more stable. All these calculation details are provided in the Electronic Supplementary Material (ESM).

3 Results and discussion

To simulate a deposit of the solid atomic B source on the Ag (111) surface, we considered the adsorption of B clusters with increasing sizes. First, a single B atom was observed to penetrate the first layer with no barrier with E_{form} of 2.02 eV (shown in Fig. S1 in the ESM). The B atom is initially located at 2 Å above the Ag (111) surface, and the total energy gradually decreases as the height decreases. The adsorption and penetration are shown with the energy profile with the distance between the B atom and substrate, where the CI-NEB calculations also confirmed that the barrier of B atomic penetration approaches zero (shown in Fig. S2 in the ESM). Similarly, the B_2 dimer adsorption would also prefer to penetrate through and be located at the second layer, with E_{form} of 1.51 eV. As observed in Fig. 1(a), the B_2 dimer would first draw the surface Ag atom up and lean on the surface. After the penetration, the Ag atom near the B_2 dimer is expelled out of its initial position, with a height difference of over 1 Å. When there is one Ag vacancy, E_{form} of B_2 is reduced to 1.45 eV.

Even the triangular B_3 determined in experiments [1] would prefer to penetrate through the first layer with E_{form} of 1.44 eV, where three nearby Ag atoms are upturned with a height difference of approximately 0.5 Å. E_{form} of B_3 is reduced from 1.44 to 1.04 eV when there is one Ag vacancy. Thus, we can expect that the initial nucleation should occur under the first layer

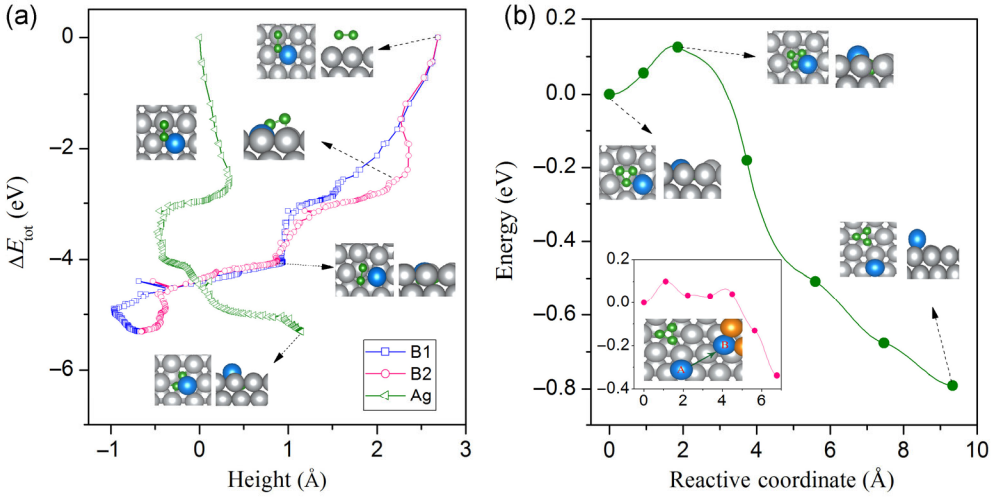

Figure 1 (Color online) Small B clusters on the Ag (111) surface. (a) Energy profiles of B_2 penetration as a function of the Ag/B heights (the position of the first Ag layer is set to zero), where green/grey atoms represent B/Ag atoms, respectively, and the expelled Ag atom is marked in blue. (b) The barrier of expelling one Ag atom to the surface; the inset shows the Ag atom diffusion on the surface with B_3 embedded in the first layer.

because the bonding between Ag and B atoms is important to stabilize the clusters. Note that Ag atoms would be expelled as more B atoms adsorb on the surface. As observed in Fig. 1(b), the barrier of one Ag atom expelled out to the surface is only 0.12 eV when there is a triangular B_3 embedded in the first layer. This Ag atom would further diffuse away on the surface easily with a diffusion barrier of 0.10 eV (shown in the inset of Fig. 1(b)).

As the number of B atoms increases, the nucleation and growth would be complicated because of the diversity of B clusters. In practice, we have considered possible triangular fragments to model the small B clusters (shown in Fig. S3 in the ESM), which were good candidates for the planar B nanostructures [23]. We have observed that the most stable B_4 is of rhombus shape with E_{form} = 1.25 eV for adsorption on the Ag (111) surface and only 1.03 eV for inside the first layer with one Ag vacancy. E_{form} of B_5 adsorption is 1.09 eV on the Ag surface, whereas it is 1.02 and 0.96 eV for the Ag surface with one and two vacancies, respectively. E_{form} of B_6 embedded in the first layer is only 0.83 eV, whereas it is 0.99 eV for adsorption on the Ag (111) surface. Thus, we can conclude that the Ag atoms would be gradually expelled and the small B clusters would be nucleated inside the first layer of Ag atoms as more B atoms are added.

Figure 2 shows the stable B nanostructures as a function of size (the detailed geometries and E_{form} values are presented in Fig. S4 in the ESM). Similar to B_4 and B_6, B_7 is the fragment of the double ring. B_9 and B_{11} are observed at the local minimum of E_{form}, corresponding to the fragments of the triple ring. Note that the stable configuration of B_{12} is of the C_{3v} symmetry as for the isolated molecular, whereas this structure embedded in the Ag surface is not a magic structure with E_{form} of 0.72 eV, larger than that of B_{11}.

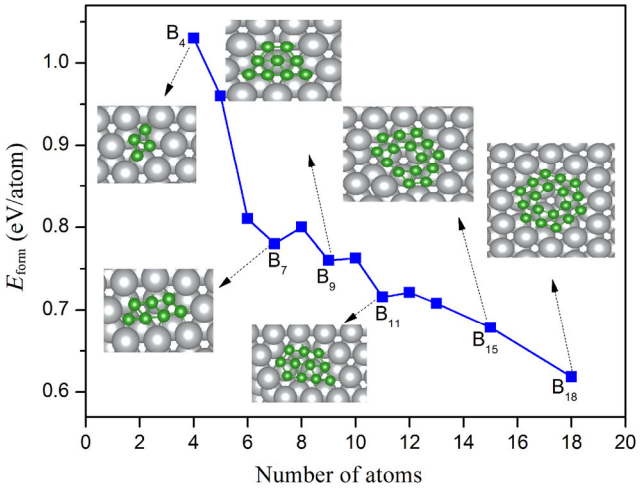

Figure 2 (Color online) Nucleation of B nanostructures inside the Ag (111) surface: E_{form} as a function of the cluster size. B_4, B_7, B_9, B_{11}, B_{15}, and B_{18} are shown as examples.

As the size increases, the structures of B_{15} and B_{18} with one vacancy are more stable. The B–Ag bonds are approximately 2.3 Å in length, and the B–Ag interaction is important for the structural stabilities of the embedded B clusters because the charge transfer would change the magic structures compared with the stable structures in the gas phase.

For the larger B nanostructures embedded in the Ag surface, we have constructed possible candidates considering the lattice match, as shown in Fig. 3(a), where the length of the B–Ag bond remains approximately 2.3 Å. There are two typical interfaces of B–Ag edges: zigzag and armchair. As verified in previous studies [5, 23], the profile shapes of isolated stable B clusters are convex with an appropriate distribution of vacancies. However, B clusters with the zigzag edge are more stable when embedded in the Ag surface. For example, E_{form} of B_{28} with two vacancies is 0.63 eV, whereas that of B_{26} with the zigzag edge is 0.60 eV. For larger structures with three vacancies, we observed that E_{form} of B_{34} with the C_{3v} symmetry is 0.64 eV, whereas that of B_{34} with the zigzag edge is 0.59 eV. In addition, E_{form} of B_{45} with the zigzag edge is 0.58 eV, whereas it is 0.63 eV when enclosed by both the zigzag and armchair edges. For simplicity, we have considered possible structures during the growth along x and y directions (shown in Fig. S5 in the ESM), where the ones with the zigzag edge are observed to be more stable compared with those with the armchair edge.

In the following part, we used the ribbons with the zigzag edge to model the growth of borophene, focusing on the vacancy concentration and distribution. For comparison, we considered three typical ribbons: the triangular fragment with no vacancy (T), I-type with vacancies in a stripe pattern (I), and II-type from the alpha-sheet (II). For example, we constructed a ribbon of B_9 (T) embedded inside the Ag surface (shown in Fig. S6 in the ESM) and observed that the structure was significantly buckled with E_{form} of 0.58 eV. The ribbon of B_8 (I) with 1/9 vacancies was observed to be stable with E_{form} of only 0.55 eV, and E_{form} of B_{25} (II) was observed to be 0.57 eV with the same width. We similarly extended the width of these types of ribbons with the number of line vacancies on the Ag surface increasing, where the I-type ribbons were more stable than the II-type ribbons with the same width (shown in Fig. S7 in the ESM). In addition, we considered the ribbon adsorption on the Ag surface without vacancies for comparison. The ribbons inside the surface were more stable for small width, and the energy difference gradually decreased with increasing width.

In general, there are many isomers with similar formation energies, and the vacancy distribution might be random initially during the nucleation. Figure 4 shows the minimum energy paths of evolution from the I-type ribbon to the II-type ribbon, where B atoms

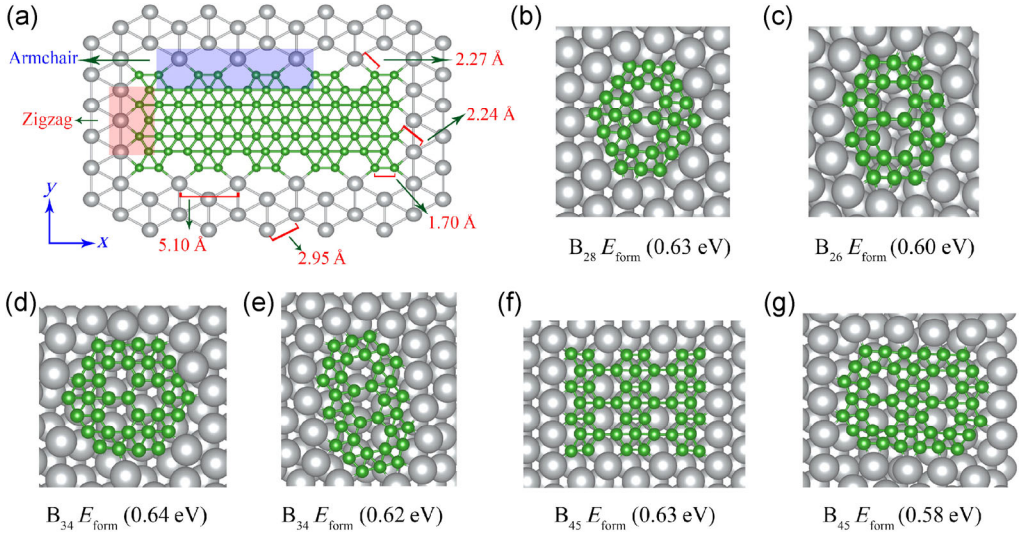

Figure 3 (Color online) Structural evolution and lattice match of B nanostructures inside the Ag (111) surface: (a) zigzag and armchair interface; (b)–(g) possible stable B nanostructures.

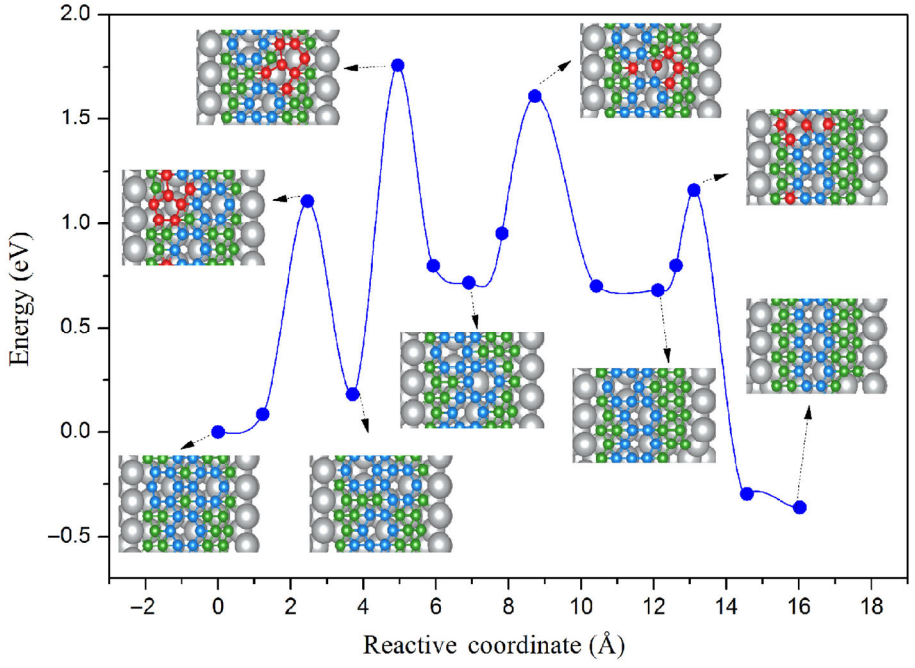

Figure 4 (Color online) Minimum energy paths of exchanging B atoms with vacancies in the B nanostructures embedded inside the Ag (111) surface. Hexagonal vacancies are marked in blue, and the pentagonal units are marked in red.

and hexagonal vacancies are exchanged. We constructed several structures with various distributions of vacancies using the isomers with low energies as intermediates. The transition states between two intermediates contain the pentagonal units and induce the reaction barriers from 0.6 to 1.6 eV. These barriers should be smaller as the size of the B nanostructures increases; thus, the migration of B atoms is probable under the experimental temperature (~1,000 K) to form a stable sheet with vacancies in a stripe pattern.

As verified above, we have demonstrated the structural evolution of B nanostructures during the nucleation, where the B–Ag bonding is important and the vacancies are necessary to enhance the stability. The ribbon with vacancies remains flat, whereas the triangular ribbon becomes buckled because of the excess electrons. Similarly, we can understand that the stable structures of B_{15} and B_{18} contain one vacancy when embedded in the Ag surface, whereas there are no vacancies for B_{16} in the gas phase. We can conclude that the stable borophene on the Ag surface should contain vacancies because the structures with vacancies are more stable in the nucleation and growth processes.

For the case of a sheet, we observed that the one with 1/6 vacancies in a stripe pattern is 0.1 eV per atom more stable than that with the triangular lattice. Figure 5 presents the simulated STM images of these two sheets for comparison. The parameters used

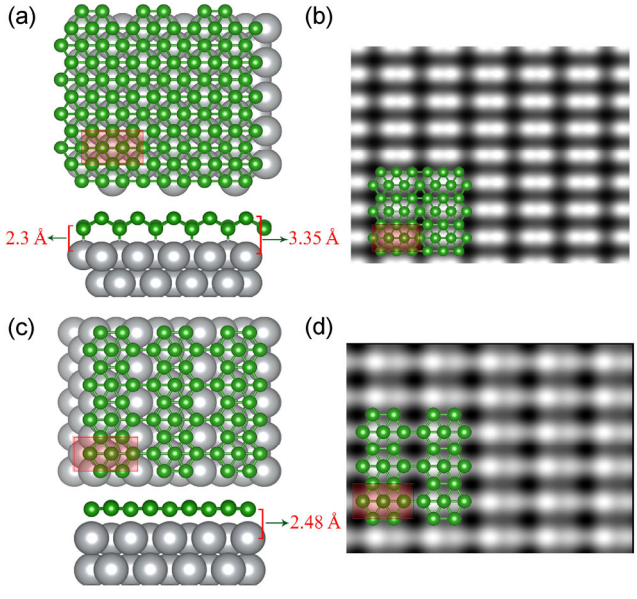

Figure 5 (Color online) STM images of borophene and the corresponding simulated empty states (V_{sample} = 1.0 V) with overlaid atomic structure: (a) and (b) triangular sheet with no vacancies and (c) and (d) sheet with 1/6 vacancies in a stripe pattern.

were the same as those used in Ref. [18], and the STM image of the buckled triangular lattice is consistent with that from Ref. [18]. Note that the STM image for the sheet with 1/6 vacancies in a stripe pattern is in better agreement with the experimental results. A recent study also confirmed the borophene with stripe vacancies using experimental and theoretical methods [24].

4 Conclusions

In summary, we theoretically investigated the formation of borophene on the Ag (111) surface. Our calculations indicate that small B clusters (B_{1-3}) deposited on the Ag surface would penetrate the first layer and further expel Ag atoms for extra B atoms. B atoms should gradually form triangular fragments on the Ag surface, where hexagonal vacancies are necessary as the cluster size increases. Because of the strong B–Ag interaction, the B clusters with the zigzag edge are stabilized, and that with vacancies in a stripe pattern would form through the probable diffusion of B atoms and vacancies. We conclude that the borophene on the Ag (111) surface should contain 1/6 vacancies in a stripe pattern, which is more energetically preferable; in addition, the corresponding STM image is in better agreement with the experimental observation.

Acknowledgements

This work was supported by National Natural Science Foundation of China (Nos. 11474100 and 11204185), Guangdong Natural Science Funds for Distinguished Young Scholars (No. 2014A030306024), and the Fundamental Research Funds for the Central Universities (Nos. 2015PT017 and 2015ZP010).

Electronic Supplementary Material: Supplementary material (calculation details, energy profiles, possible structures in the nucleation and growth of borophene) is available in the online version of this article at http://dx.doi.org/10.1007/s12274-016-1148-0.

References

[1] Sergeeva, A. P.; Popov, I. A.; Piazza, Z. A.; Li, W. L.; Romanescu, C.; Wang, L. S.; Boldyrev, A. I. Understanding boron through size-selected clusters: Structure, chemical bonding, and fluxionality. *Acc. Chem. Res.* **2014**, *47*, 1349–1358.

[2] Oger, E.; Crawford, N. R. M.; Kelting, R.; Weis, P.; Kappes, M. M.; Ahlrichs, R. Boron cluster cations: Transition from planar to cylindrical structures. *Angew. Chem., Int. Ed.* **2007**, *46*, 8503–8506.

[3] Gonzalez Szwacki, N.; Sadrzadeh, A.; Yakobson, B. I. B_{80} fullerene: An *ab initio* prediction of geometry, stability, and electronic structure. *Phys. Rev. Lett.* **2007**, *98*, 166804.

[4] Li, W. L.; Zhao, Y. F.; Hu, H. S.; Li, J.; Wang, L. S. $[B_{30}]^-$: A quasiplanar chiral boron cluster. *Angew. Chem., Int. Ed.* **2014**, *53*, 5540–5545.

[5] Piazza, Z. A.; Hu, H. S.; Li, W. L.; Zhao, Y. F.; Li, J.; Wang, L. S. Planar hexagonal B_{36} as a potential basis for extended single-atom layer boron sheets. *Nat. Commun.* **2014**, *5*, 3113.

[6] Tang, H.; Ismail-Beigi, S. Novel precursors for boron nanotubes: The competition of two-center and three-center bonding in boron sheets. *Phys. Rev. Lett.* **2007**, *99*, 115501.

[7] Yang, X. B.; Ding, Y.; Ni, J. *Ab initio* prediction of stable boron sheets and boron nanotubes: Structure, stability, and electronic properties. *Phys. Rev. B* **2008**, *77*, 041402.

[8] Penev, E. S.; Bhowmick, S.; Sadrzadeh, A.; Yakobson, B. I. Polymorphism of two-dimensional boron. *Nano Lett.* **2012**, *12*, 2441–2445.

[9] Yu, X.; Li, L. L.; Xu, X.-W.; Tang, C.-C. Prediction of two-dimensional boron sheets by particle swarm optimization algorithm. *J. Phys. Chem. C* **2012**, *116*, 20075–20079.

[10] Wu, X. J.; Dai, J.; Zhao, Y.; Zhuo, Z. W.; Yang, J. L.; Zeng, X. C. Two-dimensional boron monolayer sheets. *ACS Nano* **2012**, *6*, 7443–7453.

[11] Tang, H.; Ismail-Beigi, S. First-principles study of boron sheets and nanotubes. *Phys. Rev. B* **2010**, *82*, 115412.

[12] Lu, H. G.; Mu, Y. W.; Bai, H.; Chen, Q.; Li, S.-D. Binary nature of monolayer boron sheets from *ab initio* global searches. *J. Chem. Phys.* **2013**, *138*, 024701.

[13] Li, W.-L.; Jian, T.; Chen, X.; Chen, T.-T.; Lopez, G.-V.; Li, J.; Wang, L.-S. The planar CoB_{18}^- cluster as a motif for metallo-borophenes. *Angew. Chem., Int. Ed.*, in press, DOI: 10.1002/anie. 201601548.

[14] Liu, H. S.; Gao, J. F.; Zhao, J. J. From boron cluster to two-dimensional boron sheet on Cu(111) surface: Growth mechanism and hole formation. *Sci. Rep.* **2013**, *3*, 3238.

[15] Liu, Y. Y.; Penev, E. S.; Yakobson, B. I. Probing the synthesis of two-dimensional boron by first-principles computations. *Angew. Chem., Int. Ed.* **2013**, *52*, 3156–3159.

[16] Zhang, Z. H.; Yang, Y.; Gao, G. Y.; Yakobson, B. I. Two-dimensional boron monolayers mediated by metal substrates. *Angew. Chem., Int. Ed.* **2015**, *54*, 13022–13026.

[17] Tai, G. A.; Hu, T. S.; Zhou, Y. G.; Wang, X. F.; Kong, J. Z.; Zeng, T.; You, Y. C.; Wang, Q. Synthesis of atomically thin boron films on copper foils. *Angew. Chem., Int. Ed.* **2015**, *127*, 15693–15697.

[18] Mannix, A. J.; Zhou, X.-F.; Kiraly, B.; Wood, J. D.; Alducin, D.; Myers, B. D.; Liu, X.-L.; Fisher, B. L.; Santiago, U.; Guest, J. R. et al. Synthesis of borophenes: Anisotropic, two-dimensional boron polymorphs. *Science* **2015**, *350*, 1513–1516.

[19] Satta, M.; Colonna, S.; Flammini, R.; Cricenti, A.; Ronci, F. Silicon reactivity at the Ag(111) surface. *Phys. Rev. Lett.* **2015**, *115*, 026102.

[20] Kresse, G.; Hafner, J. *Ab initio* molecular dynamics for liquid metals. *Phys. Rev. B* **1993**, *47*, 558–561.

[21] Kresse, G.; Furthmüller, J. Efficient iterative schemes for *ab initio* total-energy calculations using a plane-wave basis set. *Phys. Rev. B* **1996**, *54*, 11169–11186.

[22] Henkelman, G.; Uberuaga, B. P.; Jónsson, H. A climbing image nudged elastic band method for finding saddle points and minimum energy paths. *J. Chem. Phys.* **2000**, *113*, 9901–9904.

[23] Xu, S.-G.; Zhao, Y.-J.; Liao, J.-H.; Yang, X.-B. Understanding the stable boron clusters: A bond model and first-principles calculations based on high-throughput screening. *J. Chem. Phys.* **2015**, *142*, 214307.

[24] Feng, B. J.; Zhang, J.; Zhong, Q.; Li, W. B.; Li, S.; Li, H.; Cheng, P.; Meng, S.; Chen, L.; Wu, K. H. Experimental realization of two-dimensional boron sheets. *Nat. Chem.* **2016**, *8*, 563–568.